# Priming of microglia in a DNA-repair deficient model of accelerated aging

Raj, Divya D. A.; Jaarsma, Dick; Holtman, Inge R.; Olah, Marta; Ferreira, Filipa M.; Schaafsma, Wandert; Brouwer, Nieske; Meijer, Michel M.; de Waard, Monique C.; van der Pluijm, Ingrid

*Published in:*
Neurobiology of Aging

*DOI:*
10.1016/j.neurobiolaging.2014.03.025

Neurobiology of Aging 35 (2014) 2147–2160

Contents lists available at ScienceDirect

Neurobiology of Aging

journal homepage: www.elsevier.com/locate/neuaging

# Priming of microglia in a DNA-repair deficient model of accelerated aging

Divya D.A. Raj [a], Dick Jaarsma [b], Inge R. Holtman [a], Marta Olah [a], Filipa M. Ferreira [b], Wandert Schaafsma [a], Nieske Brouwer [a], Michel M. Meijer [a], Monique C. de Waard [c], Ingrid van der Pluijm [c], Renata Brandt [c], Karim L. Kreft [d,e], Jon D. Laman [d], Gerald de Haan [f], Knut P.H. Biber [a,g], Jan H.J. Hoeijmakers [c], Bart J.L. Eggen [a], Hendrikus W.G.M. Boddeke [a,*]

[a] Department of Neuroscience, Section Medical Physiology, University of Groningen, University Medical Center Groningen, Groningen, the Netherlands
[b] Department of Neuroscience, Erasmus University Medical Center, Rotterdam, the Netherlands
[c] Department of Genetics, Cancer Genomics Center, Erasmus University Medical Center, Rotterdam, the Netherlands
[d] Department of Immunology, Erasmus University Medical Center and MS Center ErasMS, Rotterdam, the Netherlands
[e] Department of Neurology, Erasmus University Medical Center, Rotterdam, the Netherlands
[f] Department of Cell Biology, European Research Institute on the Biology of Aging, University of Groningen, University Medical Center, Groningen, the Netherlands
[g] Department of Psychiatry and Psychotherapy, University Medical Center, Freiburg, Germany

ARTICLE INFO

*Article history:*
Received 21 November 2013
Received in revised form 21 March 2014
Accepted 23 March 2014
Available online 28 March 2014

*Keywords:*
Microglia
Priming
Aging
DNA damage
Phagocytosis
Neuroinflammation
Neuron-glia interaction
Hyperactivation

ABSTRACT

Aging is associated with reduced function, degenerative changes, and increased neuroinflammation of the central nervous system (CNS). Increasing evidence suggests that changes in microglia cells contribute to the age-related deterioration of the CNS. The most prominent age-related change of microglia is enhanced sensitivity to inflammatory stimuli, referred to as priming. It is unclear if priming is due to intrinsic microglia ageing or induced by the ageing neural environment. We have studied this in *Ercc1* mutant mice, a DNA repair-deficient mouse model that displays features of accelerated aging in multiple tissues including the CNS. In *Ercc1* mutant mice, microglia showed hallmark features of priming such as an exaggerated response to peripheral lipopolysaccharide exposure in terms of cytokine expression and phagocytosis. Specific targeting of the *Ercc1* deletion to forebrain neurons resulted in a progressive priming response in microglia exemplified by phenotypic alterations. Summarizing, these data show that neuronal genotoxic stress is sufficient to switch microglia from a resting to a primed state.


## 1. Introduction

Microglia, the resident central nervous system (CNS) myeloid cell population, are the most prominent immune cells in the brain. It is well known that microglia in the aged brain show specific changes like enhanced sensitivity to proinflammatory stimuli (Henry et al., 2009; Norden and Godbout, 2013; Sierra et al., 2007). Such a hyper-responsive state is called priming and is viewed as a phenotype with a lower threshold to "switch" to a proinflammatory state (Lull and Block, 2010). Priming of microglia in the aged brain may result from chronic proinflammatory cues of the aging environment and is suggested to impair neuronal function and may underlie or promote neurodegeneration (Lull and Block, 2010; Norden and Godbout, 2013; Ransohoff and Perry, 2009).

Accumulation of nuclear DNA damage has been proposed as a critical factor for aging (Hoeijmakers, 2009). Genotoxic stress resulting from DNA damage accumulation evokes cell cycle checkpoint responses (Jackson and Bartek, 2009; Zhou et al., 2001) leading to cell cycle arrest and senescence (Matheu et al., 2007). DNA damage induces the expression of immune-stimulatory surface ligands and increased secretion of proinflammatory cytokines (Rodier et al., 2009) by senescent cells. This process most likely activates inflammatory pathways and immune responses that

* Corresponding author at: Department of Neuroscience, Section Medical Physiology, University of Groningen, University Medical Center Groningen, Antonius Deusinglaan 1, 9713 AV Groningen, the Netherlands. Tel.: +31 (0)50 363 2701.
*E-mail address:* h.w.g.m.boddeke@umcg.nl (H.W.G.M. Boddeke).

0197-4580/$ – see front matter © 2014 Elsevier Inc. All rights reserved.
http://dx.doi.org/10.1016/j.neurobiolaging.2014.03.025

target senescent cells in aging tissues for removal (Rodier and Campisi, 2011). In mice, DNA damage has been suggested to induce a phenotype in postmitotic neurons resembling cellular senescence and the number of senescent-like neurons increased with age (Jurk et al., 2012). Also, DNA damage has been shown to occur as part of normal brain activity (Suberbielle et al., 2013) and during brain aging (Dorszewska and Adamczewska-Goncerzewicz, 2004; Hamilton et al., 2001).

A causal relationship between accumulating DNA damage and age-related neurodegeneration has recently been suggested in *Ercc1* mutant mice (*Ercc1*$^{\Delta/-}$) that are deficient in DNA repair. In *Ercc1*$^{\Delta/-}$ mice, a decrease in neuronal synaptic plasticity, deficits in learning behavior, and deterioration of neurons has been reported in addition to considerable glial activation, findings analogous to physiological aging (Borgesius et al., 2011). Ercc1, together with XPF, forms an endonuclease essential for nucleotide excision repair (NER) (Houtsmuller et al., 1999). In addition, Ercc1 is also involved in double-strand break repair (Ahmad et al., 2008) and interstrand cross-link repair (Bergstralh and Sekelsky, 2008). In addition to DNA damage accumulation, the defects seen in *Ercc1*$^{\Delta/-}$ mice might also be the consequence of perturbed RNA polymerase II transcription initiation as it has been shown that Ercc1 is involved in RNA polymerase II assembly on promoters (Kamileri et al., 2012). We have used the *Ercc1*$^{\Delta/-}$ mouse model to determine if genotoxic stress and transcriptional blockage in neurons leads to microglial priming and if so, is microglia "switching" to a primed state the result of intrinsic damage or the consequence of perturbed neuron–glia interaction. Here we report that the *Ercc1*$^{\Delta/-}$ mutation resulted in pronounced microglia priming, reflected by enhanced endotoxin sensitivity. Furthermore, selective targeting of the Ercc1-deficiency to forebrain neurons was sufficient to "switch" microglia to a primed state; strongly suggesting that neuronal dysfunction as a result of genotoxic stress is sufficient to prime microglia.

## 2. Methods

### 2.1. Generation and breeding of mutant mice

All experiments were approved by the Institutional Animal Care and Use Committee of the University of Groningen and the Erasmus University Medical Center Rotterdam, in accordance to the Dutch animal care and use laws. The generation and characterization of nucleotide excision repair-deficient *Ercc1*$^{\Delta/+}$ and *Ercc1*$^{-/+}$ mice has been previously described (Weeda et al., 1997). *Ercc1*$^{\Delta/-}$ mice were obtained by crossing *Ercc1*$^{-/+}$ with *Ercc1*$^{\Delta/+}$ mice of C57Bl6J and FVB backgrounds to yield *Ercc1*$^{\Delta/-}$ mutants in a C57Bl6J/FVB F1 hybrid background. Wild-type (WT) littermates of the same genetic background, age, and sex were used as controls. The C57BL6J/FVB hybrid background prevents characteristics like blindness on an FVB background or deafness on a C57BL6J background. Unless specified, we used *Ercc1*$^{\Delta/-}$ mice aged 16 weeks and of both sexes for the experiments with age/sex matched genetic controls. For conditional mutant studies, an *Ercc1* allele flanked by loxP sites was used (floxed *Ercc1*, *Ercc1*$^{f/f}$; Doig et al., 2000). The αCamk2 promoter was used as a Cre driver (Tsien et al., 1996a, 1996b) and expression of this promoter is specific for postmitotic excitatory neurons (Madisen et al., 2010). *Camk2-Cre/Ercc1*$^{f/-}$ mice were obtained by crossing *Ercc1*$^{f/f}$ (FVB) with *Camk2-Cre/Ercc1*$^{+/-}$ mice (C57BL6J). As controls, *Camk2-Cre/Ercc1*$^{f/+}$ littermates were used. *hGFAP-Cre* mice were used for *Ercc1* deletion in astrocytes (Zhuo et al., 2001). Mice were housed in individually ventilated cages with ad libitum access to water and standard mouse food (CRM pellets, SDS BP Nutrition Ltd; gross energy content 18.36 kJ/g dry mass, digestible energy 13.4 kJ/g) and received liquefied food in case of motor disabilities.

### 2.2. Histologic staining and morphometric analysis

Animals were transcardially perfused under pentobarbital anesthesia with saline followed by 4% paraformaldehyde. Brains were post fixed for 24 hours, equilibrated in 25% sucrose solution, and cryosectioned at 40 μm for regular immunohistochemistry or 80 μm for morphometric analysis. For blocking and incubation steps involving antibodies, 0.3% Triton X-100 (Merck, Darmstadt, Germany) in PBS was used. Antigen retrieval (for Iba1-Mac2 co-staining) was done in 0.01 M citrate buffer (pH 6.0), followed by heating in a household microwave device at 800 W for 18 minutes. For CD68 staining, the sections were preincubated in 25 mM citrate buffer, pH 8.6, at 80 °C, for 1 hour. Following the blocking step sections were incubated in primary antibody overnight. The primary antibodies used are Iba1 (Wako, Japan), Mac2 (Cedarlane, Canada), Ki67 (Dako Cytomation, Eindhoven, the Netherlands), and CD68 (Dako Cytomation, Eindhoven, the Netherlands). As secondary antibodies, Alexafluor 488 (Molecular probes, Oregon, USA) and Cy3 (Jackson Immuno Research, Palo alto, USA) conjugated antibodies were used. The sections were mounted on gelatin (Merck)-poly-L-lysine (Sigma, Zwijndrecht, the Netherlands) coated glass slides and embedded in Mowiol (Calbiochem, Zwijndrecht, the Netherlands).

For morphometric analysis, confocal images of microglia were made with a 63× objective on a Leica SP2 confocal laser-scanning microscope at 1-μm intervals along the z-axis. Confocal images were then deconvoluted using Huygens professional imaging software (SVI). Topology of the branching cell was reconstructed in 3 dimensions and measurements quantified after retracing with the help of the Filament Tracer function of the Imaris 7.0 software (Bitplane). Care was taken that the analyzed cell within the frame was cropped (75–200 μm range) according to the extent of branches that were clearly connected to the cell body of interest and fully separable from crossing branches of other cells. Statistical analysis of the quantified measures was performed using multivariate analysis of covariance (MANCOVA) as the cellular parameters studied can influence each other. For Ki67 staining, 3 sections were counted per mouse ($n = 3$), after which the counted values were divided for the area analyzed (3–6 $mm^2$) to obtain cells/square mm. Asterisks indicate $p$-value $< 0.05$ with 1-tailed unpaired $t$-tests.

### 2.3. Acute isolation of microglia from adult mouse brain

Animals were sacrificed by means of transcardial saline perfusion under inhalation anesthesia with isoflurane and/or oxygen. The brains were isolated and kept in ice-cold medium A (HBSS containing 0.6 % glucose and 15 mM HEPES buffer). From the collected tissue microglia were isolated at high purity (>98%) using a discontinuous Percoll gradient as described previously (De Haas et al., 2007) at 4 °C. Briefly, the tissue was mechanically dissociated to form a single cell suspension (Glass potter, Braun Melsungen, Germany). After centrifugation (10 minutes, 220$g$), the cell pellet was subjected to density gradient separation using Percoll solutions with different densities. Isotonic Percoll solution (100%, density 1123 g/mL), 9 volume parts of Percoll (density 1.13 g/mL, GE Healthcare, Uppsala, Sweden, 17–0891) were mixed with one volume part of 10× HBSS. Percoll solutions with various percentages were prepared via dilution of 100% Percoll with 1× PBS. The cell pellet was resuspended in 75% Percoll, overlaid with 25% Percoll, and finally with PBS and centrifuged at a force of 800$g$ for 25 minutes. After centrifugation, microglia were collected from the 75%–25% Percoll interface, washed with PBS, and pelleted by centrifugation. The cell pellet was resuspended in culture medium (DMEM containing 5% FCS, 1% penicillin and/or streptomycin, and 1% sodium pyruvate) for functional assays. For RNA isolation, the

microglia pellet was resuspended in 20 mL Percoll solution with a density of 1.03 g/mL (40 mL myelin gradient buffer, 11.7 mL Percoll, and 1.3 mL 1.5 M NaCl). A gradient was prepared by overlaying with PBS and centrifuged at 950*g* for 20 minutes. The resulting cell pellet was separated from myelin and cell debris and stained for flow cytometry with antibodies against CD11b and CD45 (see Section 2.4 for details).

### 2.4. Flow cytometry

Cells from either the 75/25 interface or the myelin gradient buffer pellet were resuspended in medium A (without phenol red) and Fc blocked with 1% anti-CD16/32 (eBiosciences, the Netherlands) for 15 minutes, stained for different surface markers for 20 minutes and washed with PBS for subsequent flow cytometric analysis. The surface expression of markers was measured with a FACSCalibur flow cytometer (Becton Dickinson) and analyzed using FloJo software. To determine the purity of the microglia preparation a small sample of the attained cell suspension was stained for CD11b and CD45 together with a live cell marker DRAQ5 (Biostatus Ltd, UK) for $CD11b^{high}/CD45^{low}/DRAQ5+$ cells (live microglia). For immunophenotyping of mouse microglia cells the following antibodies were used: phycoerythrin (PE) coupled rat anti-mouse CD11b (Clone M1/70, eBiosciences), fluorescein isothiocyanate coupled rat anti-mouse CD45 (Clone 30-F11, eBiosciences), PE coupled rat anti-mouse TREM2b (Clone 237920, R&Dsystems), fluorescein isothiocyanate coupled rat anti-mouse CD14 (Clone Sa2-8, eBiosciences) and PE coupled rat anti-mouse CD36 (Clone 72-1, eBiosciences).

### 2.5. Lipopolysaccharide injections

Animals were intraperitoneally injected with 1 mg/kg lipopolysaccharide (LPS) (*Escherichia coli* 0111:B4; Sigma-Aldrich, St Louis, MO, USA; L4391) or saline. Three (for RNA isolation) or 18 (for immunohistochemistry) hours after injection, the animals were sacrificed and the brains were dissected and processed as described previously. Subsequently, $CD11b^{high}/CD45^{low}$ cells were sorted in RNA lysis buffer (Qiagen, Germany) for real time PCR analysis.

### 2.6. Analysis of microglia priming by quantitative real time PCR

RNA was extracted using the RNeasy Micro kit and concentrations were determined with a NanoDrop (ND1000). Complementary DNA was synthesized using RevertAid M-MuLV Reverse Transcriptase, Ribolock RNase Inhibitor, and M-MLV buffer (all Fermentas GmbH, Germany). The PCR reaction contained iQ SYBR Green Supermix (Bio-Rad) and was performed on an ABI 7900HT machine (Applied Biosystems). The primers were designed with NCBI Primer Blast software and ordered from Biolegio, the Netherlands. Supplementary Table 1 contains the list of primers used in the study.

### 2.7. Phagocytosis assay

After isolation, cells were resuspended in culture medium, seeded in 8 well Lab-Tek II Chambered Coverglass (Nunc) at a density of 5000 cells per well and allowed to attach for 20 minutes. Two hours after seeding, the medium was replaced with culture medium containing 25 μg/mL of pHrodo E. coli BioParticles conjugate (Life technologies, Molecular probes, USA). The cells were subsequently imaged for 18 hours with a Solamere Nipkow spinning disc confocal laser scanning microscope mounted on a Leica DM IRE2 inverted microscope equipped with a Stanford Photonics XR/Mega-10I (intensified) CCD camera and an ASI MS2000 Piezo motorized stage, (37 °C and 5% $CO_2$). To excite pHrodo, the 568 nm laser line of a dynamic Krypton laser was used. During image acquisition, an HC PL APO CS 10× dry objective was used. A bright field and a red channel image (pHrodo emission) were acquired every 5 minutes at each condition. Multiple cells were selected as regions of interest based on the bright field images. At the end of the imaging session, cells were stained with Syto13 (Life Technologies), an indicator for cell viability. Syto13-positive cells were selected for quantification. The intensity of the regions of interest in the red channel images was measured in each frame of the entire image stack with the help of an ImageJ plug in (written by K. Sjollema; Microscopy Center, University Medical Center Groningen, University of Groningen). The data were plotted as a time versus intensity, and the time needed to reach half maximum response for each cell was determined.

### 2.8. Determination of reactive oxygen species production

Production of reactive oxygen species by acutely isolated microglia was determined by detecting the conversion of non-fluorescent $H_2$DCFDA (2′,7′-dichlorodihydrofluorescein diacetate; Life Technologies) into fluorescent DCF (2′,7′-dichlorofluorescein) with flow cytometry. Cell suspension (100 μL) containing $2 \times 10^4$ cells was incubated, with or without $H_2$DCFDA for 20 minutes at 37 °C in polystyrene FACS tubes, after which fluorescence was determined using flow cytometry. Since the reagent is prone to oxidation, precautions were taken to prepare suspensions just before the experiment and no wash steps were used. Cells treated with vehicle (DMSO) or 40 nM adenosine triphosphate were used as negative and positive controls, respectively. The mean fluorescence intensity of DCF after subtraction of the background fluorescent values from negative controls was plotted for the indicated conditions.

### 2.9. Transcriptional profiling and network analysis

Microglia were sorted (see Section 2.4 for details) from 16 $Ercc1^{\Delta/-}$ and control mice aged 4-month-old and RNA was isolated with the Qiagen RNeasy Kit. RNA quality and concentration was assessed with a BioRad Bioanalyzer. After amplification (Nugen Ovation RNA amplification kit), RNA was labeled and hybridized to Illumina mouse-ref8 V2.0 expression beadchip microarrays. Genomestudio (version 1.9.0) was used to generate raw expression values, which were preprocessed and analyzed by project R (version 2.15.1) and BioConductor package Limma (version 1.8.18).

Transcriptional profiling was followed by Weighted Gene Co-expression Network Analysis (WCGNA) (Langfelder and Horvath, 2008). WCGNA defines co-expression relationships between all pairs of genes in the transcriptional data set resulting in a network of interconnected genes. Groups of genes that exhibit similar behavior across the data set can be identified as modules. WGCNA was performed using a soft-power (β) value of 4, based on scale free criteria. Genes with low topological overlap were filtered from the analysis resulting in a network of the 2.904 most connected genes. Only modules that significantly associated to the genotype were used for further analysis. Genes were ordered according to their module membership to generate gene lists (kME; Korrelation Module EigenGene-table) ranking genes by intramodular connectivity (Zhang and Horvath, 2005). Genes in modules often share common regulatory mechanisms or are involved in related cellular functions (Dewey et al., 2011; Langfelder et al., 2013; Mason et al., 2009; Winden et al., 2009). The Benjamini Hochberg multiple testing corrected *p*-value was generated by the p.adjust function of R-package

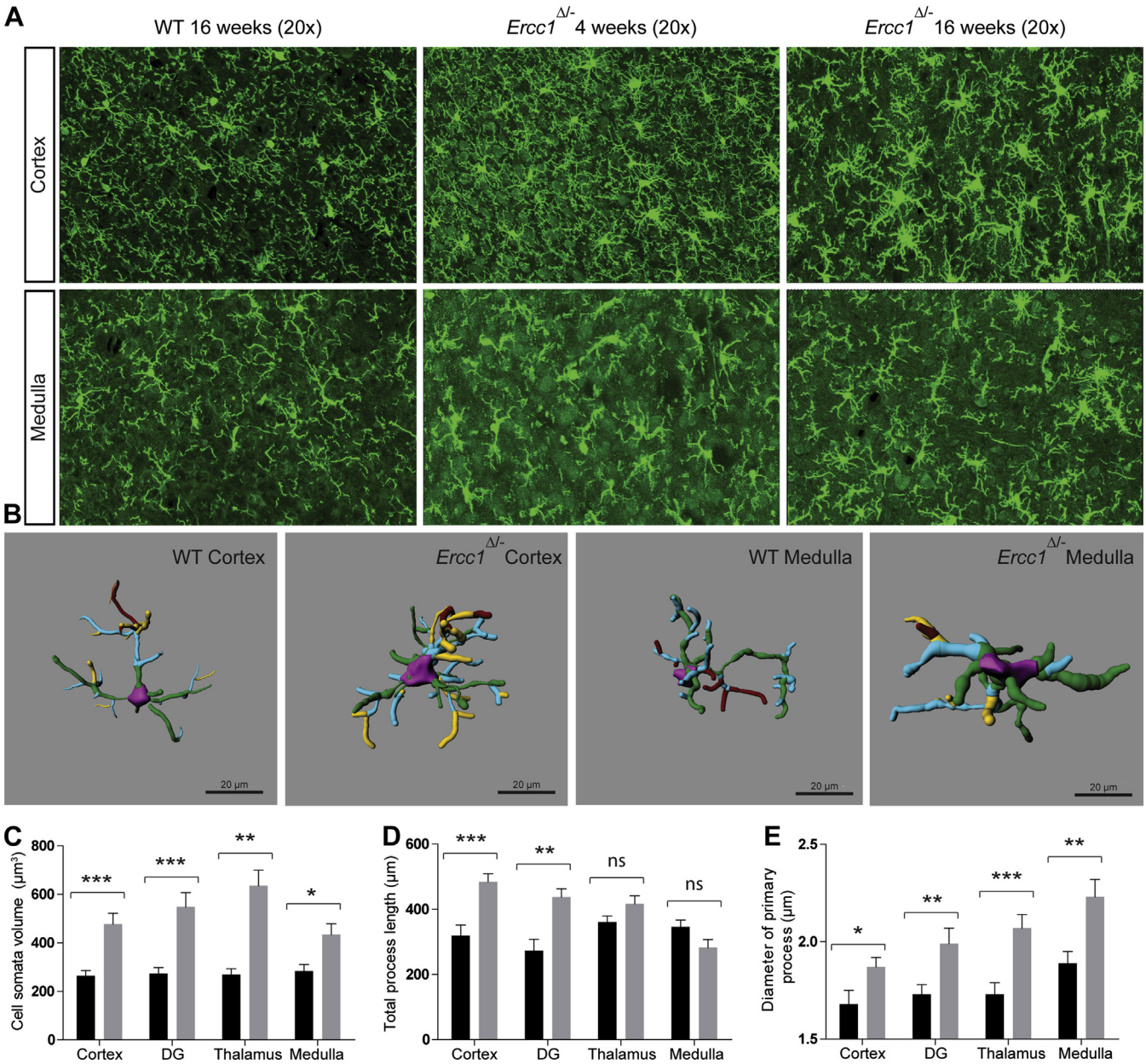


**Fig. 1.** Quantitative morphology analysis of *Ercc1*$^{\Delta/-}$ microglia. (A) Microglia morphology in cortex and medulla of WT and *Ercc1*$^{\Delta/-}$ brain. Morphology in 4- and 16-week-old WT brain is similar, only 16-week-old brains are depicted. (B) Confocal reconstruction of WT and *Ercc1*$^{\Delta/-}$ microglia (16 weeks) from cortex and medulla (scale bar = 20 µm). Analyses of morphologic parameters from WT and *Ercc1*$^{\Delta/-}$ microglia (16 weeks; black = WT, gray = *Ercc1*$^{\Delta/-}$) in cortex, dentate gyrus (DG), thalamus, and medulla of (C) total cell soma volume (D) total length of processes, and (E) diameter of primary processes in individual microglia, revealed that *Ercc1*$^{\Delta/-}$ microglia have larger cell body size, process length, and thickened primary processes compared with WT microglia (n = 30) reconstructed cells from each region from 3 WT and *Ercc1*$^{\Delta/-}$ mice. Statistical analysis was performed with an MANCOVA analysis, * $p < 0.05$; ** $p < 0.01$; *** $p < 0.005$ and ns is not significant. Abbreviations: *Ercc1*$^{\Delta/-}$, *Ercc1* mutant mice; MANCOVA, multivariate analysis of covariance; WT, wild type.

Stats. Genes from the kME-table, with a Benjamini Hochberg adjusted *p* value below 0.01 were used as input for ingenuity pathway analysis (IPA). Heatmaps were generated using heatmap.2 function of Bioconductor Package gplots 3.86 software (Hu et al., 2008).

### 2.10. Statistical analyses

MANCOVA is a statistical method to cover cases where there is more than one dependent variable and where the control of covariates is required. A covariate represents a source of variation that has not been controlled in the experiment and is believed to affect the dependent variable. For instance, in analysis of cellular morphology, thickening of processes might alter process length. MANCOVA statistical design can "factor out" the error introduced by such covariants thereby showing if individual parameters are altered. We therefore used this statistic method for quantitative morphometric analysis. Ki67 proliferation data were analyzed using 1-tailed unpaired *t*-tests. All other experiments used 1-way or multiple-way analysis of variance, followed by post hoc analysis with Bonferroni test (GraphPad Prism 5). In the figures, the *p*-value of the analysis of variance, and the post hoc tests are indicated. Graphs show both the distribution of the individual values, the resulting mean, and the standard error of the mean (SEM).

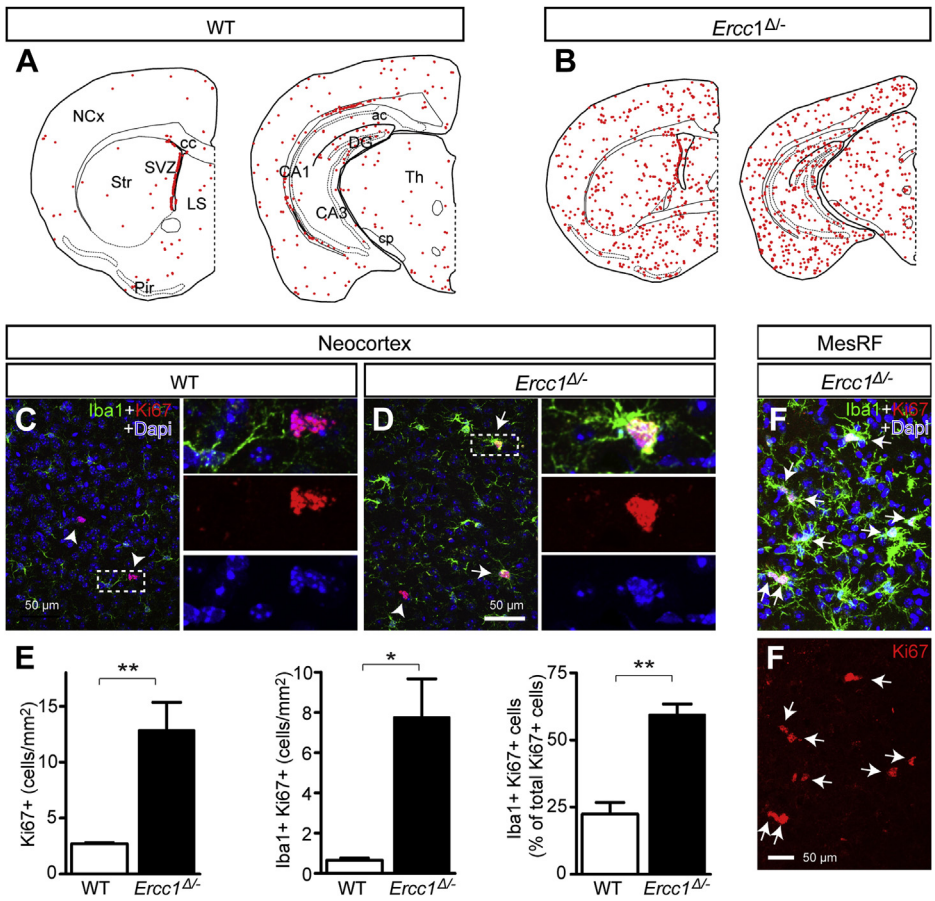


**Fig. 2.** Increase in microglia number in *Ercc1*$^{\Delta/-}$ mice. Staining of Ki67 positive cells in (A) 16-week-old WT and (B) *Ercc1*$^{\Delta/-}$ brains showed a higher number of proliferating cells in *Ercc1*$^{\Delta/-}$ with a uniform distribution throughout the brain. In WT brain, proliferating cells are predominantly located in the subventricular zone (SVZ). Proliferating cells in WT (C) and *Ercc1*$^{\Delta/-}$ (D) mice were microglia based on Ki67 (red) and Iba1 (green) co-expression; nuclei were counterstained with DAPI (blue). Quantitatively, Ki67 positive cells were increased in *Ercc1*$^{\Delta/-}$ brains. Scale bars are 50 µm. (E) Ki67-positive microglia per surface area, or as a percentage of total proliferating cells, were increased in *Ercc1*$^{\Delta/-}$ brain. In the brain stem of *Ercc1*$^{\Delta/-}$ mice, most Ki67-positive cells were Iba1-positive microglia (F; indicated by white arrows). Scale bar is 10 µm. * $p < 0.05$; ** $p < 0.01$. Abbreviations: ac, anterior commissure; CA1/CA3, corn ammonis 1/3; cc, corpus callosum; cp, cerebral crus; DG, dentate gyrus; *Ercc1*$^{\Delta/-}$, *Ercc1* mutant mice; LS, lateral septal nucleus; NCx, neocortex; Pir, piriform cortex; Str, striatum; Th, thalamus; WT, wild type. (Please refer to *Neurobiology of Aging* online for color reproduction.)

## 3. Results

### 3.1. Age-dependent changes in microglia morphology in Ercc1$^{\Delta/-}$ mice

Neuropathological visualization of local microglial morphology has been used to infer central nervous system distress (Streit et al., 1999, 2000). To investigate the effect of DNA repair deficiency-associated aging on microglia morphology, sections from *Ercc1*$^{\Delta/-}$ mice and WT littermates were stained for the microglia marker Iba1 at the age of 4 and 16 weeks. At 4 weeks, minor alterations in microglia morphology in the cortex were observed, whereas in the medulla, changes in microglia morphology were more pronounced (Fig. 1A). Differences in microglial morphology between WT and *Ercc1*$^{\Delta/-}$ mice were apparent at the age of 16 weeks throughout the brain including the cortex and medulla. Using confocal microscopy, followed by 3D reconstruction, microglia morphologies in WT and *Ercc1*$^{\Delta/-}$ mice were compared. In WT brain, microglia extended thin ramified processes, whereas in *Ercc1*$^{\Delta/-}$ mice microglia possessed hypertrophic, thickened processes, and enlarged cell bodies (Fig. 1B).

Morphometric quantification revealed that *Ercc1*$^{\Delta/-}$ microglia had a significantly increased cell soma volume in all brain regions analyzed (frontal cortex, dentate gyrus, thalamus, and medulla; Fig. 1C). The total process length of *Ercc1*$^{\Delta/-}$ microglia was longer than WT in the cortex and dentate gyrus but not in the thalamus and medulla (Fig. 1D). The primary processes in *Ercc1*$^{\Delta/-}$ microglia were significantly thickened in all brain areas tested (Fig. 1E). The degree of ramification, quantified by pseudo-coloring different levels of branching and counting of the number of segments at each level, was not significantly different between *Ercc1*$^{\Delta/-}$ and WT mice (Supplementary Fig. 1). The observed morphologic changes resemble previously reported microglia phenotypes referred to as "hypertrophic" (Ayoub and Salm, 2003; Streit, 2000), "reactive" (Gomide et al., 2005), or "intermediate" (Karperien et al., 2013).

### 3.2. Increased microglia proliferation in Ercc1$^{\Delta/-}$ mice

In *Ercc1*$^{\Delta/-}$ mice a pronounced increase in microglia was observed. To confirm that the observed increased number of microglia was because of increased proliferation, the number of proliferating cells was determined using Ki67 staining. In WT brain, most proliferating cells were localized to the neurogenic niches; note the high density of Ki67$^{+}$ cells in the sub-ventricular zone (Fig. 2A), where the *Ercc1*$^{\Delta/-}$ brain contained much more Ki67$^{+}$ cells with no apparent regional distribution (Fig. 2B) although occasional hotspots with a high density of Ki67$^{+}$ cells were noticed frequently in the brain stem (Fig. 2F). The number of Ki67$^{+}$ cells/mm$^{2}$ was

about 4-fold higher in *Ercc1*$^{\Delta/-}$ compared with WT brain (Fig. 2E). Most Ki67$^{+}$ cells in these regions were microglia, indicated by co-staining with Iba1 (Fig. 2F). Quantitative analysis indicated a 10-fold increase in the number of Ki67-Iba1 positive cells in the neocortex (Fig. 2C–E). When represented as percentage of the total number of proliferating cells, microglia constituted two-thirds of the total number of proliferating cells in the *Ercc1*$^{\Delta/-}$ brain.

### 3.3. Enhanced sensitivity of Ercc1$^{\Delta/-}$ microglia to LPS stimulation

Morphologically hypertrophic microglia can be functionally primed or activated. It is possible to differentiate between these states as primed cells do not (yet) express high amounts of inflammatory cytokines but are hypersensitive to inflammatory stimuli (Ramaglia et al., 2012; Sierra et al., 2007). To further substantiate possible immune priming, the proinflammatory response of microglia in *Ercc1*$^{\Delta/-}$ mice was studied after intraperitoneal LPS injection. Three hours after LPS injection, microglia were isolated and transcript levels were determined using quantitative reverse transcription polymerase chain reaction. Basal expression levels of cytokines IL-1β, TNFα, and IL6 were similar in WT and *Ercc1*$^{\Delta/-}$ mice. IL-1β, IL-6, and TNFα expression were induced by LPS, notably, this increase in expression was much more pronounced in *Ercc1*$^{\Delta/-}$ microglia (Fig. 3A–C). Expression levels of the typical anti-inflammatory cytokine IL-10 were comparable between WT and *Ercc1*$^{\Delta/-}$ microglia both under basal conditions and after LPS stimulation (Fig. 3D). TGF-β expression was reduced in *Ercc1*$^{\Delta/-}$ mice (~2-fold) and is induced to comparable expression levels as WT by LPS (Fig. 3E). A potential interaction between genotype and LPS treatment was assessed using a general linear model-multivariate test. A significant interaction between genotype and LPS treatment was observed the proinflammatory cytokines IL-1β, TNFα, IL6, and anti-inflammatory cytokine TGF-β. (Supplementary Table 2).

Interestingly, expression of MHC-II, reported to be important for microglia immune activation and antigen presentation (Benveniste et al., 2001; Town et al., 2005) was not detected in *Ercc1*$^{\Delta/-}$ mice (Supplementary Fig. 2). LPS hypersensitivity of *Ercc1*$^{\Delta/-}$ microglia was further substantiated by the co-staining with Iba1 and Mac-2, a marker for microglia activation. In WT animals, Mac-2 was not detected under basal conditions and only a small number of Mac-2 expressing Iba1$^{+}$ cells were observed after LPS stimulation. In *Ercc1*$^{\Delta/-}$ mice, the number of Mac-2 expressing microglia was higher than in WT mice and significantly induced by LPS, an observation further supporting a primed microglia phenotype in *Ercc1*$^{\Delta/-}$ mice (Fig. 3F). In summary, *Ercc1*$^{\Delta/-}$ microglia display an exaggerated proinflammatory response, indicative of a "primed" state and Mac-2 expression marks a subpopulation of microglia that switched to an inflammatory state and is responsive to inflammatory stimuli.

### 3.4. Ercc1$^{\Delta/-}$ microglia display increased phagocytosis and reactive oxygen species (ROS) production

Removal of cellular debris by phagocytosis is an essential function of microglia, which might change upon aging. It is unknown if primed and resting microglia have similar functional capacities. Microglia phagocytic activity was determined using pHrodo-coupled *E. coli* bioparticles. Fluorescence emission by pHrodo was plotted over time for 40 WT and *Ercc1*$^{\Delta/-}$ microglia from 3 different

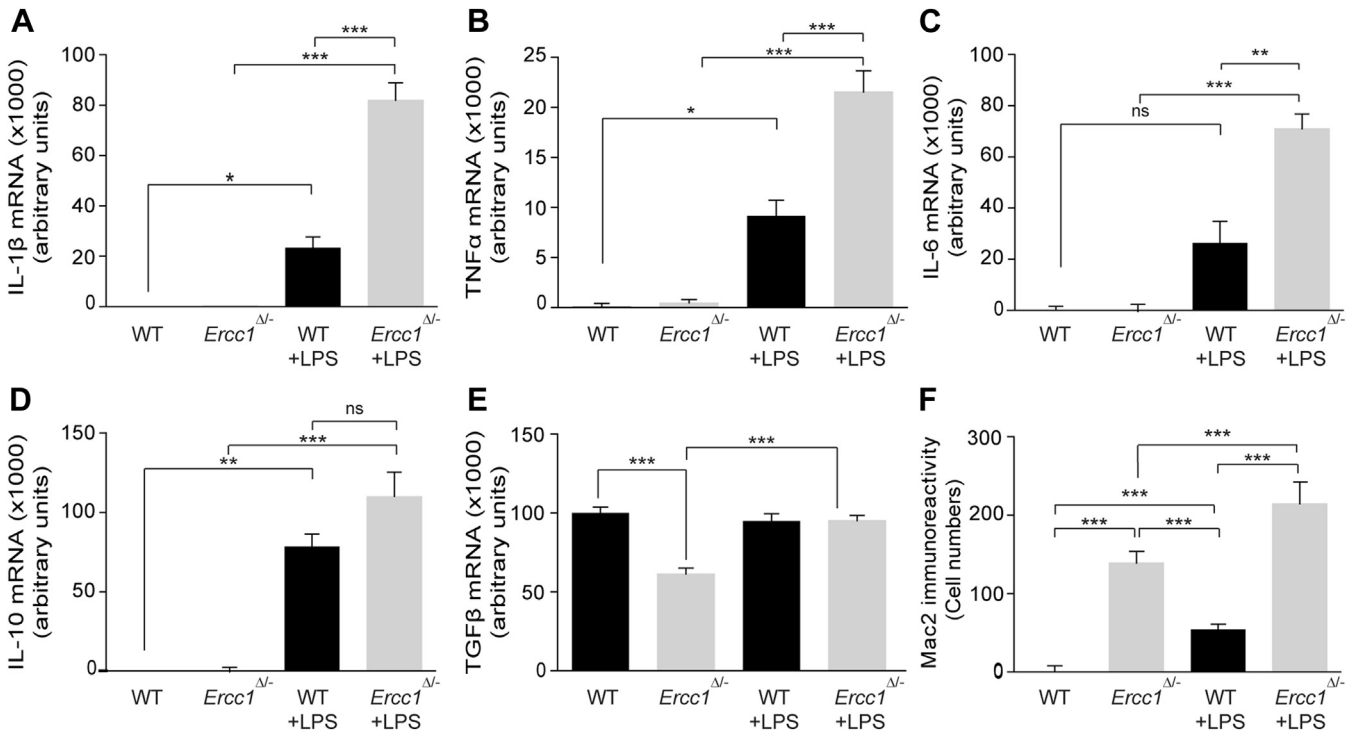


**Fig. 3.** Increased cytokine and Mac-2 expression of *Ercc1*$^{\Delta/-}$ microglia after peripheral LPS challenge. Microglia were sorted from WT and *Ercc1*$^{\Delta/-}$ mice (16 weeks), after intraperitoneal injection with PBS or LPS (1 mg/kg, 3 hours) and relative mRNA expression levels were determined by quantitative RT-PCR. Expression of proinflammatory cytokines IL-1β (A), TNFα (B), and IL-6 (C) was significantly increased in response to LPS with a much higher expression in *Ercc1*$^{\Delta/-}$ microglia compared to WT microglia. Microglia from WT and *Ercc1*$^{\Delta/-}$ mice had comparable basal anti-inflammatory IL-10 (D) expression levels and in response to LPS. Basal TGFβ (E) expression in *Ercc1*$^{\Delta/-}$ microglia was almost half of WT microglia, which was restored to WT levels after LPS injection. The number of Mac2 expressing cells (F) was higher in *Ercc1*$^{\Delta/-}$ brains compared with WT mice, even after LPS injection. The number of Mac-2 expressing cells was further increased in *Ercc1*$^{\Delta/-}$ brains upon LPS injection. * $p < 0.05$, ** $p < 0.005$, *** $p < 0.001$, and ns: not significant. Abbreviations: *Ercc1*$^{\Delta/-}$, *Ercc1* mutant mice; LPS, lipopolysaccharide; mRNA, messenger RNA; WT, wild type.

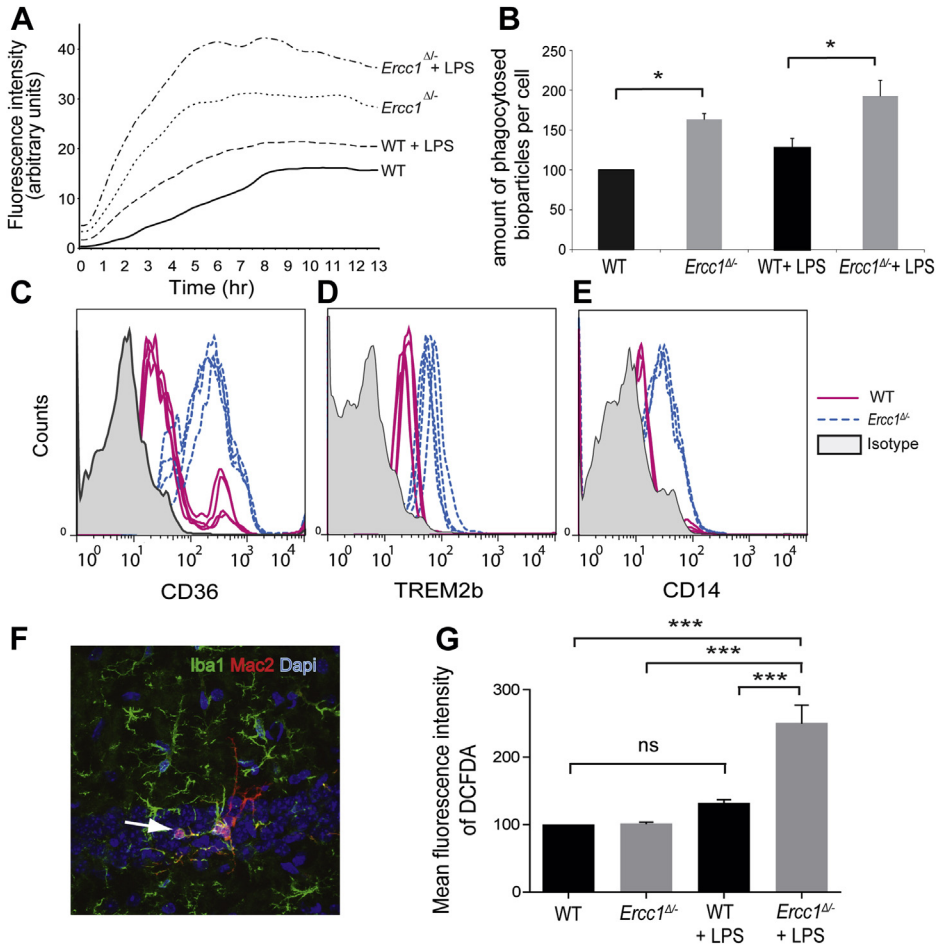


**Fig. 4.** Enhanced phagocytosis and ROS production by *Ercc1*$^{\Delta/-}$ microglia. (A) Acutely isolated microglia were incubated with pHrodo-coupled *Escherichia coli* and pHrodo fluorescence is plotted against time (in hours). *Ercc1*$^{\Delta/-}$ microglia have a higher rate of phagocytic uptake compared with WT microglia, which is further increased by LPS. (B) At the end of the experiment (13 hours), total fluorescence per cell (40 cells per category) was plotted with WT set at 100%, showing higher phagocytic intake by *Ercc1*$^{\Delta/-}$ microglia; which was further enhanced by LPS; * $p < 0.05$. *Ercc1*$^{\Delta/-}$ microglia express increased levels of phagocytic receptors CD36 (C) TREM2b (D) and CD14 (E) as measured by flow cytometry; gray-filled histograms depict isotype controls. (F) Mac2-positive *Ercc1*$^{\Delta/-}$ microglia engulfing a cell in the hippocampus. (G) Increased reactive oxygen species production by *Ercc1*$^{\Delta/-}$ compared with WT microglia acutely isolated from LPS stimulated mice. *** $p < 0.0001$; ns: not significant, 1-way ANOVA. Abbreviations: ANOVA, analysis of variance; *Ercc1*$^{\Delta/-}$, *Ercc1* mutant mice; LPS, lipopolysaccharide; ROS, reactive oxygen species; WT, wild type.

mouse preparations (Fig. 4A and B). In addition, the phagocytic activity of microglia isolated from WT and *Ercc1*$^{\Delta/-}$ mice injected with LPS (1 mg/kg body weight) was determined. *Ercc1*$^{\Delta/-}$ microglia showed significantly increased phagocytic activity compared with WT microglia (Fig. 4B) and peripheral LPS injection further increased phagocytosis of pHrodo coupled *E. coli* bioparticles, which was more pronounced in *Ercc1*$^{\Delta/-}$ microglia.

As *Ercc1*$^{\Delta/-}$ microglia displayed enhanced phagocytic activity, the expression of phagocytic receptors CD36, TREM2b, and CD14 was determined. Increased expression of these phagocytic receptors was observed in *Ercc1*$^{\Delta/-}$ microglia in vivo (Fig. 4C–E). In addition, cell engulfment was observed by Mac2-positive microglia in *Ercc1*$^{\Delta/-}$ mice suggesting active phagocytic intake in vivo (Fig. 4F). Production of reactive oxygen species (ROS) by microglia was measured using flow cytometric measurement of 2′,7′-dichlorofluorescein diacetate (DCFDA) fluorescence. Under basal conditions, no significant difference in ROS production between WT and *Ercc1*$^{\Delta/-}$ microglia was observed. However, upon peripheral LPS injection, a significant increase in ROS production was observed in *Ercc1*$^{\Delta/-}$ microglia (Fig. 4G). Summarizing, these results show increased phagocytosis and ROS production in *Ercc1*$^{\Delta/-}$ microglia, and this increase is further enhanced by LPS, suggesting that primed microglia are functionally hyper-responsive.

### 3.5. Transcriptional profile of primed microglia

To determine the gene expression profile of primed microglia, RNA from pure FACS-sorted WT and *Ercc1*$^{\Delta/-}$ microglia was isolated and hybridized to Illumina expression arrays. Co-expression network analysis was used to identify gene networks associated with microglia priming. Weighted gene co-expression network analysis (WGCNA) was applied to construct a gene co-expression network of microglia in *Ercc1*$^{\Delta/-}$ mice. After filtering lowly connective genes, a network of 2904 genes was generated. Two co-expression networks were identified with significant differential expression between WT and *Ercc1*$^{\Delta/-}$ mice (Fig. 5A). Kruskall Wallis nonparametric 1-way analysis of variance was used to calculate between group differences (the blue module: $p = 6.7 \times 10^{-6}$, yellow module: $p = 2.9 \times 10^{-5}$). The genes in the blue module are upregulated in *Ercc1*$^{\Delta/-}$ microglia, and the genes in the yellow module are downregulated in *Ercc1*$^{\Delta/-}$ microglia (Fig. 5B). These up and downregulated gene modules were combined in a module membership or kME-table and used as input for IPA. IPA showed that the following immune-related signaling pathways were upregulated in *Ercc1*$^{\Delta/-}$ microglia, particularly communication between innate and adaptive immune cells, antigen presentation, complement system, role of pattern recognition receptors, activation of microglia, and

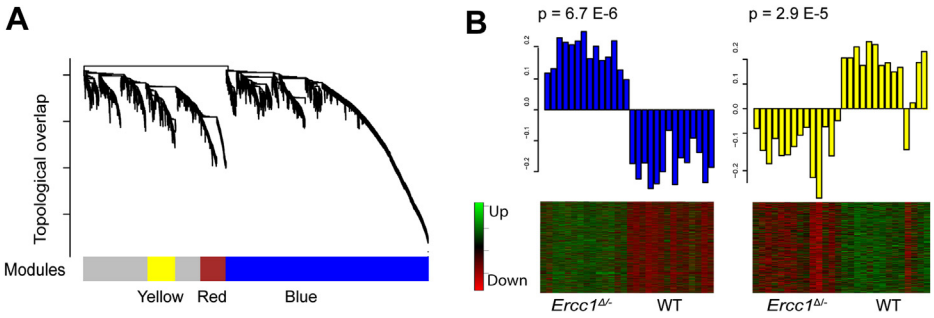


C

| Pathways | p-value | Ratio |
|---|---|---|
| EIF2-signaling | 4.3 E-26 | 0.27 |
| Antigen presentation | 8.1 E-8 | 0.36 |
| Complement system | 1.4 E-6 | 0.30 |
| Pattern Recognition Receptors | 1.6 E-6 | 0.16 |
| Interferon signaling | 1.7 E-4 | 0.23 |
| Chemokine signaling | 6.9 E-3 | 0.11 |

D

| Functions | p-value | Z | Nr |
|---|---|---|---|
| Cell migration | 2.4 E-14 | 4.32 | 96 |
| Inflammatory response | 8.9 E-12 | 3.73 | 64 |
| Adhesion of immune cells | 5.2 E-9 | 4.23 | 34 |
| Activation of microglia | 1.3 E-7 | 1.47 | 15 |
| Phagocytosis | 7.3 E-6 | 2.28 | 22 |

**Fig. 5.** Network and pathway analysis of microarray data from *Ercc1*$^{\Delta/-}$ microglia. (A) Dendrogram and associated gene modules. The dendrogram is produced by average linkage hierarchical clustering of genes based on topological overlap. Modules were assigned colors as indicated in the horizontal bar below the dendrogram. (B) Bar graphs and heatmaps showing the blue and yellow module EigenGene (first principal component, a representative of the module) and the associated genes expression values. Tables show canonical pathways (C) or biological functions (D) from ingenuity pathway analysis significantly increased in *Ercc1*$^{\Delta/-}$ microglia. Abbreviation: *Ercc1*$^{\Delta/-}$, *Ercc1* mutant mice. (Please refer to *Neurobiology of Aging* online for color reproduction.)

interferon signaling (Fig. 5C). Also a significant increase in several other IPA functions such as cell migration, inflammatory response, adhesion of immune cells, activation of microglia, phagocytosis was observed in *Ercc1*$^{\Delta/-}$ microglia (Fig. 5D). Taken together, network and pathway analyses indicated an enhanced immune state of *Ercc1*$^{\Delta/-}$ microglia with a clear phagocytic and chemotactic profile.

### 3.6. *Microglial priming is induced by genotoxic stress in* Ercc1$^{\Delta/-}$*-targeted forebrain neurons*

Mac-2 has been shown to be expressed by activated microglia (Rotshenker, 2009) and in the *Ercc1*$^{\Delta/-}$ brains, Mac-2 was found to be expressed in a "switched" microglia subpopulation. To determine the localization and distribution of these switched cells, brain sections from 16-week-old WT and *Ercc1*$^{\Delta/-}$ mice were co-stained for Iba1 and Mac-2. In WT mice, Iba1-positive microglia displayed a resting (highly ramified, small cell soma) phenotype and no Mac-2 positive microglia were found (Fig. 6A–D, insets are enlarged in panels E and F). In *Ercc1*$^{\Delta/-}$ mice, Iba$^{+}$ microglia displayed an altered morphology (also see Fig. 1, thickened processes, enlarged soma), with extensive co-expression of Mac-2 (Fig. 6G–J; insets are enlarged in panels K and L). Mac2 immunoreactivity was restricted to Iba1$^{+}$ cells and most pronounced in white matter tracts including the corpus callosum and the anterior commissure. Also the brain stem, particularly the mesencephalic reticular formation (MesRF), contained extensive Mac-2 positive microglia. This observation, in combination with the notion that particularly neurons suffer from DNA-damage accumulation (Borgesius et al., 2011), led us to hypothesize that genotoxic damage to neurons resulted in the observed microglia priming and activation. To determine if the observed morphologic changes and Mac2 expression by microglia indeed were induced by genotoxic stress in neurons, the *Ercc1*$^{f/-}$ deletion was specifically targeted to CamK2-expressing forebrain neurons (*CamK2-Cre/Ercc1*$^{f/-}$) and to GFAP-expressing astrocytes (*GFAP-Cre/Ercc1*$^{f/-}$). Detailed characterization of generic *Ercc1*$^{\Delta/-}$ mice revealed that microglia priming and activation was observed in all brain regions and that the intensity of priming-associated hypertrophy was much more pronounced in the medulla compared with the cortex (Fig. 1). The neocortex of *Ercc1*$^{\Delta/-}$ mice showed robust microglial hypertrophy (Fig. 7B, magnified image in G) in comparison to control mice with the same genetic background (*Ercc1*$^{+/+}$; Fig. 7A). Microglia hypertrophy was much more pronounced in the brain stem (MesRF) of generic *Ercc1*$^{\Delta/-}$ mice (Fig. 7J) and while Mac-2 expression was rarely detected in the cortex of *Ercc1*$^{\Delta/-}$ mice, the medulla showed abundant Mac-2 expression (compare Fig. 7, panels G and J) possibly indicating more extensive "switching" of microglia in the hindbrain. In *Camk2-Cre/Ercc1*$^{f/-}$ mice, microglia hypertrophy and Mac2 immunoreactivity were restricted to the neocortex (Fig. 7D, magnified image in I), whereas no microglia hypertrophy or Mac-2 expression was observed in hindbrain regions of *Camk2-Cre/Ercc1*$^{f/-}$ mice (Fig. 7L) or in *Camk2-Cre/Ercc1*$^{f/+}$ control mice (Fig. 7K). This showed that priming microglia (based on an hypertrophic morphology and Mac-2 expression) was restricted to the region of forebrain neurons targeted by the *Camk2-Cre* transgene. In the GFAP-targeted *Ercc1*$^{f/-}$ mice, no microglial hypertrophy or Mac2 expression was observed (Fig. 7F) indicating that DNA damage accumulation in astrocytes did not induce microglia hypertrophy or priming. Microglia priming was further substantiated by CD68 expression in the cortex of 16-week-old control and *Ercc1*$^{\Delta/-}$ mice and 26-week-old *Camk2-Cre/Ercc1*$^{f/-}$ mice (Fig. 7M–O).

A time-course of microglia priming was determined in forebrain sections of 8, 16, and 26-week-old *Camk2-Cre/Ercc1*$^{f/-}$ mice (Fig. 8). An age-dependent change in microglia morphology and increase in Iba1 intensity was observed in *Camk2-Cre/Ercc1*$^{f/-}$ mice (Fig. 8A–D). Both in lamina II/III and V, a primed microglia morphology was first observed at week 16 and more pronounced at 26 weeks (Fig. 8E–L). Mac-2/Iba1 co-expression was first observed after 26 weeks (Fig. 8A–L). Interestingly, at 8 weeks, clusters of tubular microglia, or rod cells, postulated to be involved in neuroprotection, appeared in lamina V of the cortex (Fig. 8J–L) (Graeber, 2010; Lambertsen et al., 2011; Wierzba-Bobrowicz et al., 2002; Ziebell et al., 2012).

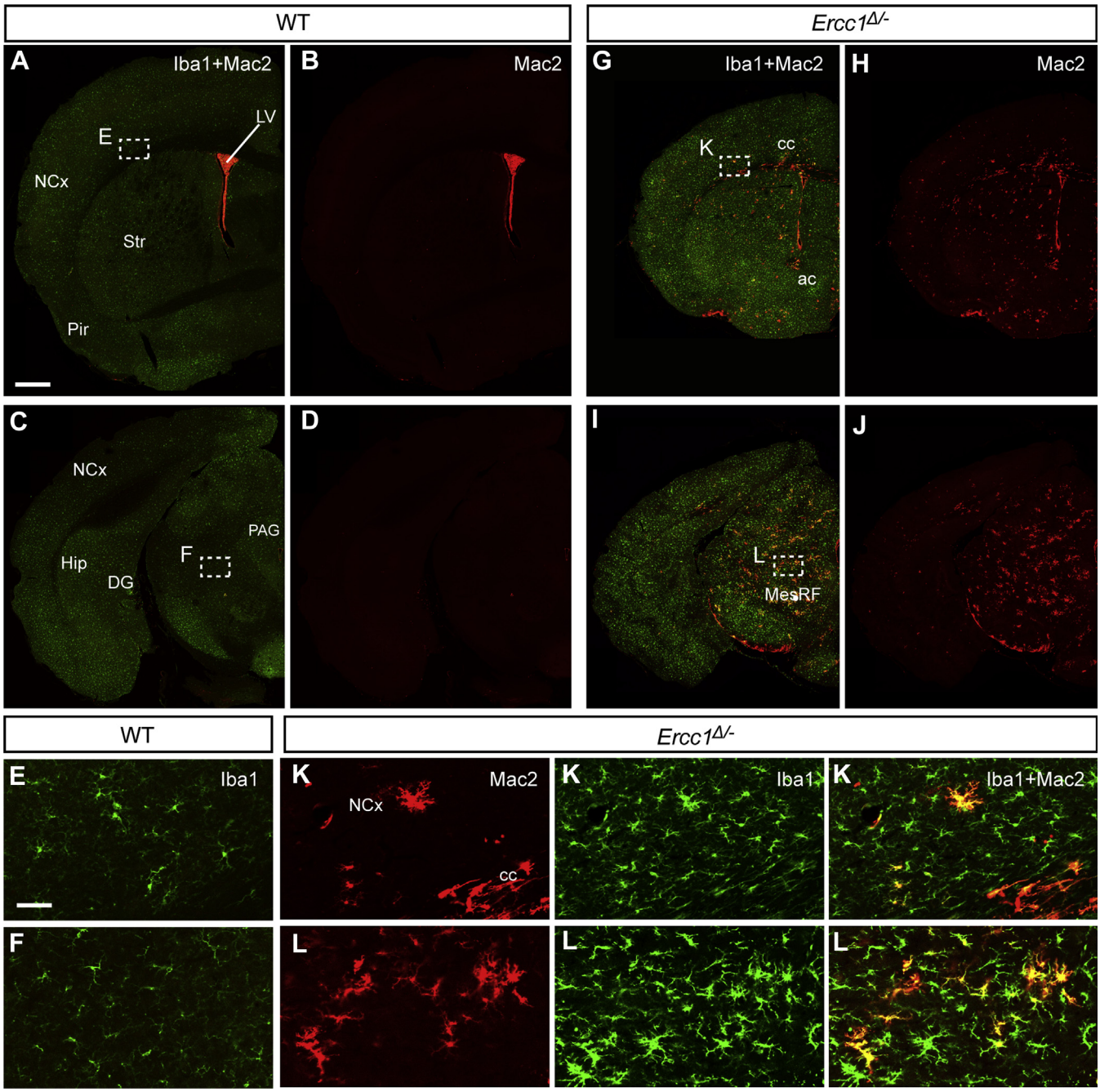


**Fig. 6.** Localization of primed microglia in *Ercc1*$^{\Delta/-}$ brains. Co-staining of 16-week-old WT (panels A–F) and *Ercc1*$^{\Delta/-}$ (panels G–L) sections with Iba1 (green) and Mac-2 (red) to identify localization and distribution of primed microglia. Mac2-positive microglia were largely found in *Ercc1*$^{\Delta/-}$ white matter tracts. Corpus callosum (cc) and anterior commissure (ac) showed several Mac2-positive microglia (panel G and inset K). Also brain stem, in particular the mesencephalic reticular formation (MesRF) contained abundant Mac2-positive microglia (panel I and inset L). The scale bar indicates 500 μm in panels A–D and G–J and 50 μm in panels E, F, K, and L. Abbreviations: ac, anterior commissure; C, cortex; DG, dentate gyrus; *Ercc1*$^{\Delta/-}$, *Ercc1* mutant mice; Hip, hippocampus; LV, lateral ventricle; NCx, neocortex; PAG, periaqueductal gray; Pir, piriform cortex; Str, striatum; WT, wild type. (Please refer to *Neurobiology of Aging* online for color reproduction.)

Summarizing, these data strongly suggest, that upon targeted ablation of *Ercc1* in forebrain neurons, local microglia acquire a morphology associated with priming in a time-dependent fashion and eventually some microglia express Mac-2, possibly indicative of a more inflammatory state.

## 4. Discussion

Microglia priming as characterized by exaggerated proinflammatory response has been shown in the aged brain (Henry et al., 2009; Sierra et al., 2007) and is associated with neurodegenerative diseases (Cunningham et al., 2009; Dantzer et al., 2008; Norden and Godbout, 2013; Perry et al., 2007). Classically in neuropathology, microglia have been categorized into a resting, ramified form and a completely de-ramified, activated form. However, a spectrum of "intermediate" morphologies exists which have been described in literature as "reactive," "intermediate," and "hypertrophic" and have been viewed as both activated as well as primed microglia (Ayoub and Salm, 2003; Beynon and Walker, 2012; Gomide et al., 2005; Hwang et al., 2008; Karperien et al.,

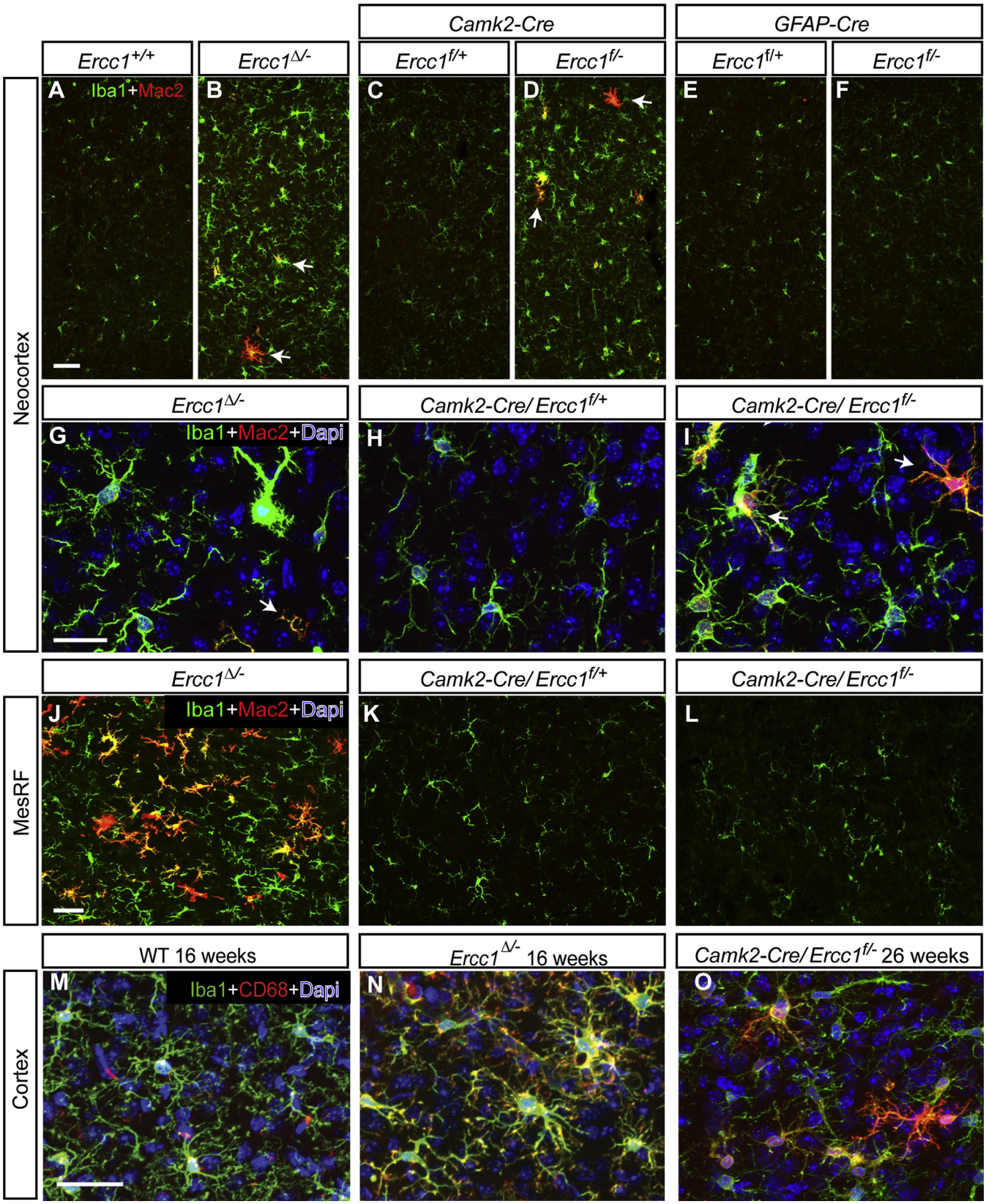


**Fig. 7.** Microglial priming response to forebrain neuron-targeted DNA repair deficiency. Sections of forebrain neuron-targeted and astrocyte-targeted Ercc1$^{f/-}$ from 26-week-old mice were co-stained for Iba1 (green) and Mac-2 (red). Microglia in transgenic control mice brains (A, C, E, H, and K) showed ramified and non-primed microglia whereas microglia in the cortex of *Camk2* targeted *Ercc1* brains (*Camk2-Cre/Ercc1*$^{f/-}$) (D, I) showed a primed hypertrophic morphology. Brain stem region of *Camk2-Cre/Ercc1*$^{f/-}$ brains (L) (which do not suffer *Ercc1* ablation) did not display microglia hypertrophy. Cortex (B, G) and brain stem (J) of 16-week-old *Ercc1*$^{\Delta/-}$ brains show hypertrophic microglia and increased Mac2 positivity. In 26-week-old astrocyte (GFAP) targeted *Ercc1*$^{-/-}$ mice (F), the cortex shows ramified, non-primed microglia comparable to its transgenic control (E). An additional marker for microglia priming, CD68 was shown to be expressed both in 16-week-old *Ercc1*$^{\Delta/-}$ mice as (N) well as in 26-week-old *Camk2-Cre/Ercc1*$^{f/-}$ mice (O). Scale bars indicate 50 μm. Abbreviation: *Ercc1*$^{\Delta/-}$, *Ercc1* mutant mice. (Please refer to *Neurobiology of Aging* online for color reproduction.)

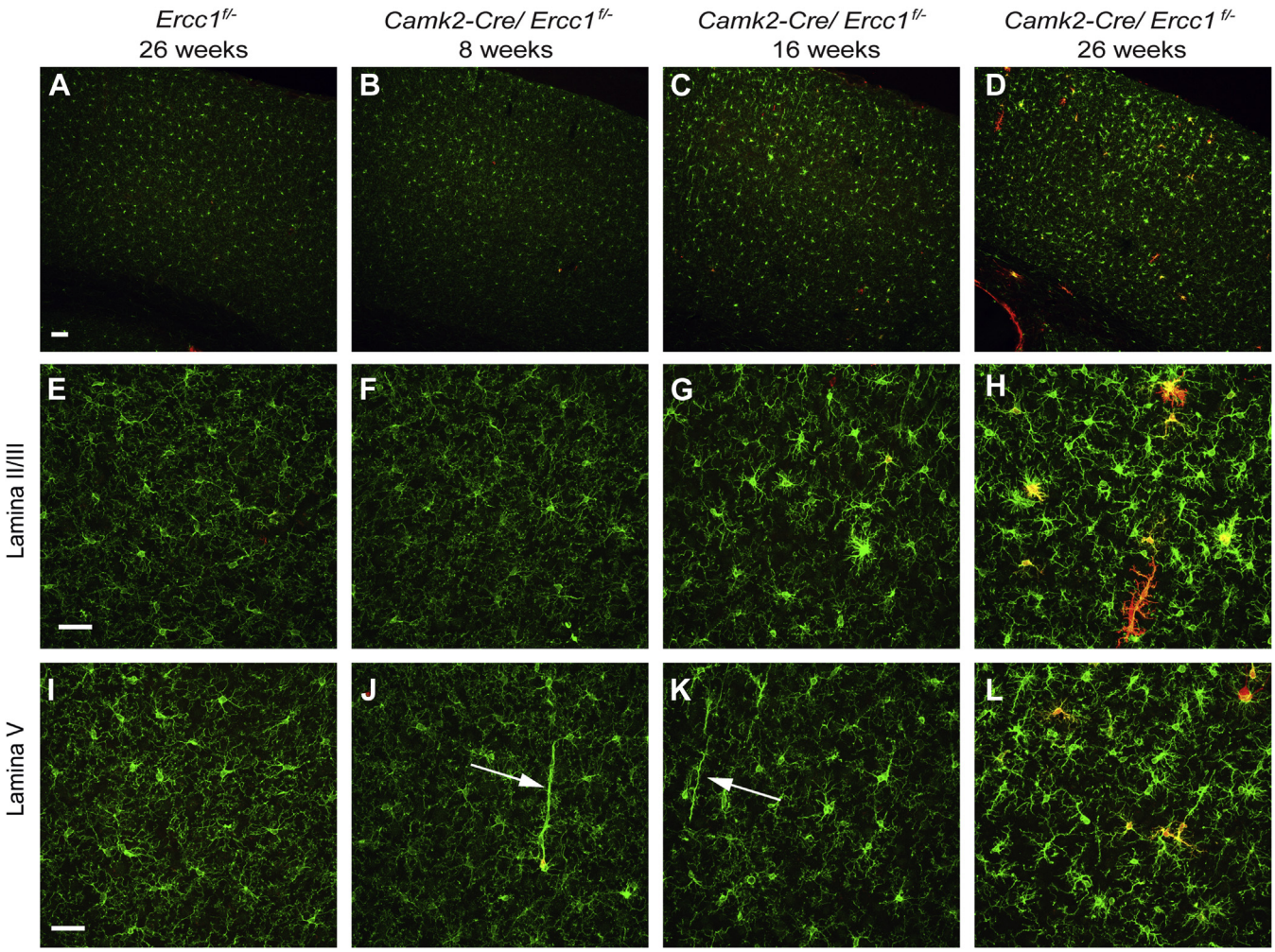


**Fig. 8.** Characterization of microglia priming in Camk2 targeted *Ercc1* mice. The time-course of microglia priming was determined in 8-, 16-, and 26-week-old *Camk2-Cre/Ercc1*$^{f/-}$ mice, compared with 26-week-old *Ercc1*$^{f/-}$ mice. The sections were co-stained for Iba1 (green) and Mac-2 (red). Panels A, B, C, and D show an overview of 26-week-old *Ercc1*$^{f/-}$ mice (A) and 8- (B), 16- (C), and 26-(D) week-old *Camk2-Cre/Ercc1*$^{f/-}$ mice, where an age-dependent increase in Iba1 intensity and changes in microglia morphology was observed. Mac-2 expression was most apparent in 26-week-old mice. Both in lamina II/III and V, a change toward a hypertrophic morphology occurred at week 16 (G, K) and was more pronounced at 26 weeks (H, L). Interestingly, at 8 and 16 weeks (J, K) long shaped clusters of so-called tubular microglia were observed in lamina V (white arrows). Scale bars indicate 50 μm. (M). Abbreviation: *Ercc1*$^{\Delta/-}$, *Ercc1* mutant mice. (Please refer to *Neurobiology of Aging* online for color reproduction.)

2013; Luo et al., 2010; Streit, 2000). Changes in microglia morphology, in correlation to altered function, have previously been shown in models of tissue injury (Davis et al., 1994; Graeber and Streit, 2010; Stence et al., 2001; Streit et al., 1999). More recently, dynamic remodeling of microglia, particularly the extent of ramification, was reported to be important in monitoring, regulating, and responding to synaptic activity in the brain (Nimmerjahn et al., 2005; Wake et al., 2009). In a model of chronic stress, microglia have been shown to respond by increasing the extent of secondary branching in the prefrontal cortex, correlating to local neuronal activity, and behavioral changes (Hinwood et al., 2012). Although it is difficult to directly link morphology to function, changes in microglia morphology are a clear indication of perturbed brain homeostasis.

*Ercc1*$^{\Delta/-}$ microglia showed a hypertrophic morphology (thickened arbors and larger cell bodies) and extensive proliferation. With digital morphometric analysis in the cortex, microglia process length increased, whereas in the medulla microglia processes were shortened. Microglial hypertrophy and enhanced responsiveness to systemic inflammation has been shown previously in a prion disease model where microglia are primed (Gómez-Nicola et al., 2013; Perry et al., 2007). Interestingly, enhanced production of proinflammatory cytokines after an inflammatory stimulation, a hallmark of microglia priming, has been reported in aged mouse microglia (Godbout et al., 2005; Sierra et al., 2007). A similar LPS hyper-responsiveness, proliferation and hypertrophy was observed in *Ercc1*$^{\Delta/-}$ microglia, indicating that microglia are primed in this model of DNA repair deficiency.

The effect of priming on microglia functionality has not been explored yet. *Ercc1*$^{\Delta/-}$ microglia showed higher expression of phagocytic receptors (Fig. 5) and show increased phagocytic activity, which was further enhanced by LPS. Furthermore, production of reactive oxygen species was enhanced in microglia upon LPS stimulation. Summarizing, the data show that primed *Ercc1*$^{\Delta/-}$ microglia display enhanced phagocytic activity and ROS production. Also, these functions are hyper-responsive to LPS. Using expression profiling and subsequent WCGNA analysis of *Ercc1*$^{\Delta/-}$-derived microglia, a priming-associated expression network was identified that contained many immune signaling related genes. Interestingly, several genes upregulated in *Ercc1*$^{\Delta/-}$ microglia are also increased in expression in physiologically aged microglia (Hickman et al., 2013).

Notably, messenger RNA (mRNA) expression of MHC-II complex encoding H2 genes was increased in *Ercc1*$^{\Delta/-}$ microglia, an

observation in agreement with data obtained in aging mice where increased CD68 and MHC II mRNA levels were observed (Godbout et al., 2005). Increased MHC II protein expression has been reported in aged human and primate brain (Dickson et al., 1992; Sheffield and Berman, 1998). Surprisingly, in *Ercc1*$^{\Delta/-}$ mice MHC-II protein expression was not detected on microglia whereas phagocytic markers like Mac2 and CD68 showed robust expression. Moreover, LPS injection in *Ercc1*$^{\Delta/-}$ mice resulted in a significant increase in the number of Iba1/Mac2 positive cells, much more than in WT mice, indicating the presence of an increased number of microglia poised to switch to an inflammatory state in *Ercc1*$^{\Delta/-}$ mice. Additionally, Mac2$^{+}$ microglia often showed phagocytic inclusions. *Ercc1*$^{\Delta/-}$ microglia therefore likely present a phenotype that is adapted to phagocytic clearance but not (yet) immune activated in the absence of an inflammatory stimulus. When stimulated, these microglia possibly switch to a proinflammatory state. However, isolation and inflammatory analysis of Mac2$^{+}$ and Mac2$^{-}$ subpopulations of microglia would be required to further substantiate this hypothesis.

Previously, it was shown that DNA damage accumulation in *Ercc1*$^{\Delta/-}$ mice primarily affected neurons and to a small extent astrocytes. Markers of genotoxic stress such as p53 and ATF3 were rarely detected in microglia (De Waard et al., 2010). We hypothesized that neuronal distress in this aging model could be the cause of the observed microglia priming. Analysis of Camk2-targeted *Ercc1*$^{f/-}$ (*Camk2-Cre/Ercc1*$^{f/-}$) mice, where DNA damage is specifically targeted to forebrain neurons showed that Mac2 and CD68 expression was restricted to the forebrain (Fig. 7). Progressive microglia priming was observed from 8 to 26 weeks in *Camk2-Cre/Ercc1*$^{f/-}$ mice. Furthermore, the morphology of primed microglia in *Camk2-Cre/Ercc1*$^{f/-}$ mice was highly similar to the morphology of *Ercc1*$^{\Delta/-}$ microglia (Fig. 8). Therefore, microglia priming (based on hypertrophic morphology and Mac2 and CD68 expression) was restricted to forebrain regions expressing the *Camk2-Cre* transgene. Although astrocytes are susceptible to DNA damage, microglia priming did not occur in astrocyte-targeted *Ercc1*$^{-/-}$ mice (De Waard et al., 2010). These observations strongly suggest that the priming response in microglia was instigated by neuronal dysfunction; it is unclear why neurons are relatively sensitive to impaired Ercc1 activity, since it is unknown which types of lesions accumulate in *Ercc1* impaired cells.

In the cortex 8- to16-week-old *Camk2-Cre/Ercc1*$^{f/-}$ mice, microglia rod cells were observed (Fig. 8). Rod cells are longitudinally shaped microglia that typically align with apical dendrites (Graeber, 2010) and have been associated with neural protection in cerebral ischemia (Lambertsen et al., 2011), Alzheimer's disease (Wierzba-Bobrowicz et al., 2002), and traumatic brain injury (Ziebell et al., 2012). Rod cells were exclusively found in the lamina of the cortex and preceded the occurrence of Mac2 expression in microglia suggesting that rod cells are the first indicators of cellular stress of pyramidal cells in lamina V. These data suggest that genotoxic stress in Camk2-targeted neurons induced microglia priming.

While accumulation of DNA damage could potentially induce a "senescence-like" state in neurons (Jurk et al., 2012), perturbed transcriptional initiation might also cause neuronal dysfunction (Barzilai et al., 2008; Brooks, 2008) and as a result trigger immune activation. Indeed, the late phase long-term potentiation stage of synaptic transmission that is dependent on mRNA transcription and protein synthesis (Kelleher et al., 2004) has been shown to be affected in *Ercc1*$^{\Delta/-}$ mice (Borgesius et al., 2011). It is likely that dysfunctional neurons affected by DNA damage communicate with microglia using several routes. While enhanced LPS reactivity has been used to characterize primed microglia in this study, the aging brain offers alternative priming triggers including complement proteins and adenosine triphosphate. In line with this reasoning, an increase in complement system activity has been previously reported in primed microglia (Eikelenboom and Veerhuis, 1996; Ramaglia et al., 2012) and increased complement gene expression was observed in *Ercc1*$^{\Delta/-}$ microglia.

The link between DNA damage events, inflammation, and tissue specific degeneration is only beginning to be understood. Interestingly, a chronic cell-autonomous inflammatory response has been shown to occur in *Ercc1*-deficient adipocytes that led to recruitment of leukocytes and ultimately resulted in adipose tissue degeneration (Karakasilioti et al., 2013). A recent study showed that loss of NF-κB signaling delayed DNA damage-induced aging and senescence (Tilstra et al., 2012). These studies suggest that DNA damage and transcriptional initiation defects-induced neuronal dysfunction could instigate an inflammatory reaction, possibly amplified by microglia in the brain, leading to the cognitive dysfunction associated with NER defects and by analogy aging. The existence and characteristics of an inflammatory phenotype in aging neurons remains to be studied.

In conclusion, our data strongly suggest that the microglial immune priming observed in this DNA repair deficient model of accelerated aging most likely is the consequence of an affected neuronal environment. The observed enhanced phagocytic activity might suggest that initially the priming response of microglia might support the degenerating brain. However, in case of persistent microglia stimulation by a degenerating brain environment or by an additional inflammatory stimulus, these primed microglia display an enhanced reactivity particularly in terms of cytokine secretion and ROS production. This might have serious implications for the extent of neurodegeneration induced by insults such as infections and stroke in segmental progeroid syndromes caused by defective NER such as xeroderma pigmentosum, Cockayne syndrome, and trichothiodystrophy. Although direct extrapolations from progeroid models to physiological aging should be treated with restraint, understanding the signaling mechanisms that lead to enhanced reactivity in microglia might also help understand priming in the naturally aging brain and reveal if microglia priming is a potential confounding factor in neurodegenerative pathologies.

## Dislosure statement

The authors have no actual or potential conflicts of interest.

## Acknowledgements

Part of the work has been performed at the UMCG microscopy and imaging center (UMIC), which is sponsored by NWO-grants 40-00506-98-9021 and 175-010-2009-023. Help with live imaging by Klaas Sjollema (UMCG) and Gert van Cappellen (Erasmus MC) is greatly acknowledged. Operators of central FACS facility of UMCG, Geert Mesander and Henk Moes are acknowledged. The authors also acknowledge advice with statistical methods by Ilia Vainchtein. This work was supported by the European commission FP7 Markage (FP7-Health-2008–200880), National Institute of Health (NIH)/National Institute of Aging (NIA) (1PO1 AG-17242-02), NIEHS (1UO1 ES011044), and the Royal Academy of Arts and Sciences of the Netherlands (academia professorship to Jan H.J. Hoeijmakers) and a European Research Council Advanced Grant to Jan H.J. Hoeijmakers. The research leading to these results has received funding from the European Community's Seventh Framework Programme (FP7/2007–2013) under grant agreement No. HEALTH-F2-2010- 259893. This work was also supported by the Mouse Clinic for Cancer and Aging through a RoadMap grant from the Netherlands Organization for Scientific Research (NWO). The

MSCenter ErasMS is supported by a program grant of the Dutch MS Research Foundation.

## Appendix A. Supplementary data

Supplementary data associated with this article can be found, in the online version, at http://dx.doi.org/10.1016/j.neurobiolaging.2014.03.025.

## References


Ahmad, A., Robinson, A.R., Duensing, A., van Drunen, E., Beverloo, H.B., Weisberg, D.B., Hasty, P., Hoeijmakers, J.H., Niedernhofer, L.J., 2008. ERCC1-XPF endonuclease facilitates DNA double-strand break repair. Mol. Cell Biol. 28, 5082–5092.

Ayoub, A.E., Salm, A.K., 2003. Increased morphological diversity of microglia in the activated hypothalamic supraoptic nucleus. J. Neurosci. 23, 7759–7766.

Barzilai, A., Biton, S., Shiloh, Y., 2008. The role of the DNA damage response in neuronal development, organization and maintenance. DNA Repair (Amst) 7, 1010–1027.

Benveniste, E.N., Nguyen, V.T., O'Keefe, G.M., 2001. Immunological aspects of microglia: relevance to Alzheimer's disease. Neurochem. Int. 39, 381–391.

Bergstralh, D.T., Sekelsky, J., 2008. Interstrand crosslink repair: can XPF-ERCC1 be let off the hook? Trends Genet. 24, 70–76.

Beynon, S.B., Walker, F.R., 2012. Microglial activation in the injured and healthy brain: what are we really talking about? Practical and theoretical issues associated with the measurement of changes in microglial morphology. Neuroscience 225, 162–171.

Borgesius, N.Z., de Waard, M.C., van der Pluijm, I., Omrani, A., Zondag, G.C., van der Horst, G.T., Melton, D.W., Hoeijmakers, J.H.J., Jaarsma, D., Elgersma, Y., 2011. Accelerated age-related cognitive decline and neurodegeneration, caused by deficient DNA repair. J. Neurosci. 31, 12543–12553.

Brooks, P.J., 2008. The 8, 5′-cyclopurine-2′-deoxynucleosides: candidate neurodegenerative DNA lesions in xeroderma pigmentosum, and unique probes of transcription and nucleotide excision repair. DNA Repair (Amst) 7, 1168–1179.

Cunningham, C., Campion, S., Lunnon, K., Murray, C.L., Woods, J.F., Deacon, R.M., Rawlins, J.N., Perry, V.H., 2009. Systemic inflammation induces acute behavioral and cognitive changes and accelerates neurodegenerative disease. Biol. Psychiatry 65, 304–312.

Dantzer, R., O'Connor, J.C., Freund, G.G., Johnson, R.W., Kelley, K.W., 2008. From inflammation to sickness and depression: when the immune system subjugates the brain. Nat. Rev. Neurosci. 9, 46–55.

Davis, E.J., Foster, T.D., Thomas, W.E., 1994. Cellular forms and functions of brain microglia. Brain Res. Bull. 34, 73–78.

De Haas, A.H., Boddeke, H.W., Brouwer, N., Biber, K., 2007. Optimized isolation enables ex vivo analysis of microglia from various CNS regions. Glia 55, 1374–1384.

De Waard, M.C., van der Pluijm, I., Zuiderveen Borgesius, N., Comley, L.H., Haasdijk, E.D., Rijksen, Y., Ridwan, Y., Zondag, G., Hoeijmakers, J.H.J., Elgersma, Y., Gillingwater, T.H., Jaarsma, D., 2010. Age-related motor neuron degeneration in DNA repair-deficient Ercc1 mice. Acta Neuropathol. 120, 461–475.

Dewey, F.E., Perez, M.V., Wheeler, M.T., Watt, C., Spin, J., Langfelder, P., Horvath, S., Hannenhalli, S., Cappola, T.P., Ashley, E.A., 2011. Gene coexpression network topology of cardiac development, hypertrophy, and failure. Circ. Cardiovasc. Genet. 4, 26–35.

Dickson, D.W., Crystal, H.A., Mattiace, L.A., Masur, D.M., Blau, A.D., Davies, P., Yen, S.H., Aronson, M.K., 1992. Identification of normal and pathological aging in prospectively studied nondemented elderly humans. Neurobiol. Aging 13, 179–189.

Doig, J., Anderson, C., Lawrence, N.J., Selfridge, J., Brownstein, D.G., Melton, D.W., 2000. Mice with skin specific DNA repair gene (*Ercc1*) inactivation are hypersensitive to ultraviolet irradiation-induced skin cancer and show more rapid actinic progression. Oncogene 25, 6229–6238.

Dorszewska, J., Adamczewska-Goncerzewicz, Z., 2004. Oxidative damage to DNA, p53 gene expression and p53 protein level in the process of aging in rat brain. Respir. Physiol. Neurobiol. 139, 227–236.

Eikelenboom, P., Veerhuis, R., 1996. The role of complement and activated microglia in the pathogenesis of Alzheimer's disease. Neurobiol. Aging 17, 673–680.

Godbout, J.P., Chen, J., Abraham, J., Richwine, A.F., Berg, B.M., Kelley, K.W., Johnson, R.W., 2005. Exaggerated neuroinflammation and sickness behavior in aged mice following activation of the peripheral innate immune system. FASEB J. 19, 1329–1331.

Gómez-Nicola, D., Fransen, N.L., Suzzi, S., Perry, V.H., 2013. Regulation of microglial proliferation during chronic neurodegeneration. J. Neurosci. 33, 2481–2493.

Gomide, V., Bibancos, T., Chadi, G., 2005. Dopamine cell morphology and glial cell hypertrophy and process branching in the nigrostriatal system after striatal 6-OHDA analyzed by specific sterological tools. Int. J. Neurosci. 115, 557–582.

Graeber, M.B., 2010. Changing face of microglia. Science 330, 783–788.

Graeber, M., Streit, W., 2010. Microglia: biology and pathology. Acta Neuropathol. 119, 89–105.

Hamilton, M.L., Van Remmen, H., Drake, J.A., Yang, H., Guo, Z.M., Kewitt, K., Walter, C.A., Richardson, A., 2001. Does oxidative damage to DNA increase with age? Proc. Natl. Acad. Sci. U.S.A 98, 10469–10474.

Henry, C.J., Huang, Y., Wynne, A.M., Godbout, J.P., 2009. Peripheral lipopolysaccharide (LPS) challenge promotes microglial hyperactivity in aged mice that is associated with exaggerated induction of both pro-inflammatory IL-1beta and anti-inflammatory IL-10 cytokines. Brain Behav. Immun. 23, 309–317.

Hickman, S.E., Kingery, N.D., Ohsumi, T.K., Borowsky, M.L., Wang, L.C., Means, T.K., El Khoury, J., 2013. The microglial sensome revealed by direct RNA sequencing. Nat. Neurosci. 16, 1896–1905.

Hinwood, M., Tynan, R.J., Charnley, J.L., Beynon, S.B., Day, T.A., Walker, F.R., 2012. Chronic stress induced remodeling of the prefrontal cortex: structural reorganization of microglia and the inhibitory effect of minocycline. Cereb. Cortex 22, 1442–1454.

Hoeijmakers, J.H.J., 2009. DNA damage, aging, and cancer. N. Engl. J. Med. 361, 1475–1485.

Houtsmuller, A.B., Rademakers, S., Nigg, A.L., Hoogstraten, D., Hoeijmakers, J.H., 1999. Action of DNA repair endonuclease ERCC1/XPF in living cells. Science 284, 958–961.

Hu, Z., Snitkin, E.S., DeLisi, C., 2008. VisANT: an integrative framework for networks in systems biology. Brief Bioinform. 9, 317–325.

Hwang, I.K., Lee, C.H., Li, H., Yoo, K.Y., Choi, J.H., Kim, D.W., Kim, D.W., Suh, H.W., Won, M.H., 2008. Comparison of ionized calcium-binding adapter molecule1 immunoreactivity of the hippocampal dentate gyrus and CA1 region in adult and aged dogs. Neurochem. Res. 33, 1309–1315.

Jackson, S.P., Bartek, J., 2009. The DNA-damage response in human biology and disease. Nature 461, 1071–1078.

Jurk, D., Wang, C., Miwa, S., Maddick, M., Korolchuk, V., Tsolou, A., Gonos, E.S., Thrasivoulou, C., Saffrey, M.J., Cameron, K., von Zglinicki, T., 2012. Postmitotic neurons develop a p21-dependent senescence-like phenotype driven by a DNA damage response. Aging Cell 11, 996–1004.

Kamileri, I., Karakasilioti, I., Sideri, A., Kosteas, T., Tatarakis, A., Talianidis, I., Garinis, G.A., 2012. Defective transcription initiation causes postnatal growth failure in a mouse model of nucleotide excision repair (NER) progeria. Proc. Natl. Acad. Sci. U.S.A 109, 2995–3000.

Karakasilioti, I., Kamileri, I., Chatzinikolaou, G., Kosteas, T., Vergadi, E., Robinson, A.R., Tsamardinos, I., Rozgaja, T.A., Siakouli, S., Tsatsanis, C., Niedernhofer, L.J., Garinis, G.A., 2013. DNA damage triggers a chronic autoinflammatory response, leading to fat depletion in NER progeria. Cell Metab. 18, 403–415.

Karperien, A., Ahammer, H., Jelinek, H.F., 2013. Quantitating the subtleties of microglial morphology with fractal analysis. Front. Cell Neurosci. 7, 3.

Kelleher 3rd, R.J., Govindarajan, A., Tonegawa, S., 2004. Translational regulatory mechanisms in persistent forms of synaptic plasticity. Neuron 44, 59–73.

Lambertsen, K.L., Deierborg, T., Gregersen, R., Clausen, B.H., Wirenfeldt, M., Nielsen, H.H., Dalmau, I., Diemer, N.H., Dagnaes-Hansen, F., Johansen, F.F., Keating, A., Finsen, B., 2011. Differences in origin of reactive microglia in bone marrow chimeric mouse and rat after transient global ischemia. J. Neuropathol. Exp. Neurol. 70, 481–494.

Langfelder, P., Horvath, S., 2008. WGCNA: an R package for weighted correlation network analysis. BMC Bioinformatics 9, 559–565.

Langfelder, P., Mischel, P.S., Horvath, S., 2013. When is hub gene selection better than standard meta-analysis? PLoS One 8, e61505.

Lull, M.E., Block, M.L., 2010. Microglial activation and chronic neurodegeneration. Neurotherapeutics 7, 354–365.

Luo, X.G., Ding, J.Q., Chen, S.D., 2010. Microglia in the aging brain: relevance to neurodegeneration. Mol. Neurodegener. 5, 12–21.

Madisen, L., Zwingman, T.A., Sunkin, S.M., Oh, S.W., Zariwala, H.A., Gu, H., Ng, L.L., Palmiter, R.D., Hawrylycz, M.J., Jones, A.R., Lein, E.S., Zeng, H., 2010. A robust and high-throughput Cre reporting and characterization system for the whole mouse brain. Nat. Neurosci. 13, 133–140.

Mason, M.J., Fan, G., Plath, K., Zhou, Q., Horvath, S., 2009. Signed weighted gene co-expression network analysis of transcriptional regulation in murine embryonic stem cells. BMC Genomics 10, 327–331.

Matheu, A., Maraver, A., Klatt, P., Flores, I., Garcia-Cao, I., Borras, C., Flores, J.M., Viña, J., Blasco, M.A., Serrano, M., 2007. Delayed ageing through damage protection by the Arf/p53 pathway. Nature 448, 375–379.

Nimmerjahn, A., Kirchhoff, F., Helmchen, F., 2005. Resting microglial cells are highly dynamic surveillants of brain parenchyma *in vivo*. Science 308, 1314–1318.

Norden, D.M., Godbout, J.P., 2013. Microglia of the aged brain: primed to be activated and resistant to regulation. Neuropathol. Appl. Neurobiol. 39, 19–34.

Perry, V.H., Cunningham, C., Holmes, C., 2007. Systemic infections and inflammation affect chronic neurodegeneration. Nat. Rev. Immunol. 7, 161–167.

Ramaglia, V., Hughes, T.R., Donev, R.M., Ruseva, M.M., Wu, X., Huitinga, I., Baas, F., Neal, J.W., Morgan, B.P., 2012. C3-dependent mechanism of microglial priming relevant to multiple sclerosis. Proc. Natl. Acad. Sci. U.S.A 109, 965–970.

Ransohoff, R.M., Perry, V.H., 2009. Microglial physiology: unique stimuli, specialized responses. Annu. Rev. Immunol. 27, 119–145.

Rodier, F., Coppé, J.P., Patil, C.K., Hoeijmakers, W.A., Muñoz, D.P., Raza, S.R., Freund, A., Campeau, E., Davalos, A.R., Campisi, J., 2009. Persistent DNA damage signalling triggers senescence-associated inflammatory cytokine secretion. Nat. Cell Biol. 11, 973–979.

Rodier, F., Campisi, J., 2011. Four faces of cellular senescence. J. Cell Biol. 192, 547–556.

Rotshenker, S., 2009. The role of Galectin-3/MAC-2 in the activation of the innate-immune function of phagocytosis in microglia in injury and disease. J. Mol. Neurosci. 39, 99–103.
Sheffield, L.G., Berman, N.E., 1998. Microglial expression of MHC class II increases in normal aging of nonhuman primates. Neurobiol. Aging 19, 47–55.
Sierra, A., Gottfried-Blackmore, A.C., McEwen, B.S., Bulloch, K., 2007. Microglia derived from aging mice exhibit an altered inflammatory profile. Glia 55, 412–424.
Stence, N., Waite, M., Dailey, M.E., 2001. Dynamics of microglial activation: a confocal time-lapse analysis in hippocampal slices. Glia 33, 256–266.
Streit, W.J., Walter, S.A., Pennell, N.A., 1999. Reactive microgliosis. Prog. Neurobiol. 57, 563–581.
Streit, W.J., 2000. Microglial response to brain injury: a brief synopsis. Toxicol. Pathol. 28, 28–30.
Suberbielle, E., Sanchez, P.E., Kravitz, A.V., Wang, X., Ho, K., Eilertson, K., Devidze, N., Kreitzer, A.C., Mucke, L., 2013. Physiologic brain activity causes DNA double-strand breaks in neurons, with exacerbation by amyloid-beta. Nat. Neurosci. 16, 613–621.
Town, T., Nikolic, V., Tan, J., 2005. The microglial 'activation' continuum: from innate to adaptive responses. J. Neuroinflammation 2, 24.
Tilstra, J.S., Robinson, A.R., Wang, J., Gregg, S.Q., Clauson, C.L., Reay, D.P., Nasto, L.A., St Croix, C.M., Usas, A., Vo, N., Huard, J., Clemens, P.R., Stolz, D.B., Guttridge, D.C., Watkins, S.C., Garinis, G.A., Wang, Y., Niedernhofer, L.J., Robbins, P.D., 2012. NF-kappaB inhibition delays DNA damage-induced senescence and aging in mice. J. Clin. Invest. 122, 2601–2612.
Tsien, J.Z., Huerta, P.T., Tonegawa, S., 1996a. The essential role of hippocampal CA1 NMDA receptor dependent synaptic plasticity in spatial memory. Cell 87, 1327–1338.
Tsien, J.Z., Chen, D.F., Gerber, D., Tom, C., Mercer, E.H., Anderson, D.J., Mayford, M., Kandel, E.R., Tonegawa, S., 1996b. Subregion- and cell type-restricted gene knockout in mouse brain. Cell 87, 1317–1326.
Wake, H., Moorhouse, A.J., Jinno, S., Kohsaka, S., Nabekura, J., 2009. Resting microglia directly monitor the functional state of synapses *in vivo* and determine the fate of ischemic terminals. J. Neurosci. 29, 3974–3980.
Weeda, G., Donker, I., de Wit, J.J., Morreau, H., Janssens, R., Vissers, C.J., Nigg, A., van Steeg, H., Bootsma, D., Hoeijmakers, J.H., 1997. Disruption of mouse Ercc1 results in a novel repair syndrome with growth failure, nuclear abnormalities and senescence. Curr. Biol. 7, 427–439.
Wierzba-Bobrowicz, T., Gwiazda, E., Kosno-Kruszewska, E., Lewandowska, E., Lechowicz, W., Bertrand, E., Szpak, G.M., Schmidt-Sidor, B., 2002. Morphological analysis of active microglia-rod and ramified microglia in human brains affected by some neurological diseases (SSPE, Alzheimer's disease and Wilson's disease). Folia Neuropathol. 40, 125–131.
Winden, K.D., Oldham, M.C., Mirnics, K., Ebert, P.J., Swan, C.H., Levitt, P., Rubenstein, J.L., Horvath, S., Geschwind, D.H., 2009. The organization of the transcriptional network in specific neuronal classes. Mol. Syst. Biol. 5, 291–309.
Ziebell, J.M., Taylor, S.E., Cao, T., Harrison, J.L., Lifshitz, J., 2012. Rod microglia: elongation, alignment, and coupling to form trains across the somatosensory cortex after experimental diffuse brain injury. J. Neuroinflammation 9, 247–251.
Zhang, B., Horvath, S., 2005. A general framework for weighted gene co-expression network analysis. Stat. Appl. Genet. Mol. Biol. 4, 17–21.
Zhou, J., Ahn, J., Wilson, S.H., Prives, C., 2001. A role for p53 in base excision repair. EMBO J. 20, 914–923.
Zhuo, L., Theis, M., Alvarez-Maya, I., Brenner, M., Willecke, K., Messing, A., 2001. hGFAP-cre transgenic mice for manipulation of glial and neuronal function in vivo. Genesis 31, 85–94.